# Inelastic neutron scattering spectrum of H2@C60 and its temperature dependence decoded using rigorous quantum calculations and a new selection rule

Minzhong Xu, Shufeng Ye, Anna Powers, Ronald Lawler, Nicholas J. Turro et al.

Citation: J. Chem. Phys. **139**, 064309 (2013); doi: 10.1063/1.4817534
View online: http://dx.doi.org/10.1063/1.4817534
View Table of Contents: http://jcp.aip.org/resource/1/JCPSA6/v139/i6
Published by the AIP Publishing LLC.

# Inelastic neutron scattering spectrum of $H_2@C_{60}$ and its temperature dependence decoded using rigorous quantum calculations and a new selection rule

Minzhong Xu,[1,2] Shufeng Ye,[2] Anna Powers,[2] Ronald Lawler,[3] Nicholas J. Turro,[4] and Zlatko Bačić[1,2,a)]

[1]*State Key Laboratory of Precision Spectroscopy and Institute of Theoretical and Computational Science, East China Normal University, Shanghai 200062, China*
[2]*Department of Chemistry, New York University, New York, New York 10003, USA*
[3]*Department of Chemistry, Brown University, Providence, Rhode Island 02912, USA*
[4]*Department of Chemistry, Columbia University, New York, New York 10027, USA*

(Received 4 June 2013; accepted 22 July 2013; published online 12 August 2013)

In the supramolecular complex $H_2@C_{60}$, the lightest of molecules, $H_2$, is encapsulated inside the most highly symmetric molecule $C_{60}$. The elegance and apparent simplicity of $H_2@C_{60}$ conceal highly intricate quantum dynamics of the coupled translational and rotational motions of the guest molecule in a nearly spherical nanoscale cavity, which embodies some of the most fundamental concepts of quantum mechanics. Here we present the first rigorous and highly accurate quantum calculations of the inelastic neutron scattering (INS) spectra of this prototypical endohedral fullerene complex and their temperature dependence. The calculations enable complete assignment of the recently reported experimental INS spectra of $H_2@C_{60}$ measured at several temperatures. We also derive a new and unexpected selection rule for the INS spectroscopy of $H_2$ in a near-spherical confinement, which explains why the INS transitions between certain translation-rotation eigenstates of $H_2$ in $C_{60}$ have zero intensity and do not appear in the spectra. © *2013 AIP Publishing LLC*. [http://dx.doi.org/10.1063/1.4817534]

## I. INTRODUCTION

The paradigmatic endohedral fullerene complex $H_2@C_{60}$ represents a felicitous union of the simplest of all molecules, $H_2$, with one of the most elegant, highly symmetric, and intellectually captivating molecules, $C_{60}$. But besides its strong esthetic appeal, $H_2@C_{60}$ has received a great deal of attention because of the profoundly quantum character of the dynamics of the entrapped $H_2$ molecule which, despite the apparent simplicity of the system, displays surprising complexity and intertwines numerous fundamental concepts of quantum mechanics.[1] The large quantum effects which dominate the translational motions of the center of mass (cm) of $H_2$ as well as the rotation of the molecule arise from the confinement of the light guest molecule inside the small $C_{60}$ cavity. For the excitation energy of 200 $cm^{-1}$, close to the translational fundamental of $H_2$ in $C_{60}$,[2] the de Broglie wavelength of the caged $H_2$, 2.4 bohrs, is comparable to the diameter of the confining space accessible in this energy range, ∼2 bohrs.[2] Consequently, the three translational degrees of freedom of the incarcerated $H_2$ are quantized due to the confinement, and their discrete eigenstates are well separated in energy, as are the quantized rotational levels of $H_2$ owing to its exceptionally large rotational constant, 7.24 meV in the ground vibrational state, inside $C_{60}$.[3] The resulting translation-rotation (TR) energy level structure is sparse. As a result, the TR, or "rattling," dynamics of the nanoconfined $H_2$ molecule is in the strongly quantum regime, i.e., it cannot be described in terms of classical mechanics, especially for the very low temperatures at which many of the spectroscopic measurements discussed below are performed.

The quantum TR dynamics of the caged $H_2$ is even more intricate due to the fact that since its two protons with the nuclear spin 1/2 are fermions, the Pauli principle requires the total molecular wave function to be antisymmetric with respect to the nuclear exchange. This gives rise to two nuclear spin isomers, para-$H_2$ (p-$H_2$) and ortho-$H_2$ (o-$H_2$), having the antisymmetric $I = 0$ and the symmetric $I = 1$ total nuclear spin states, respectively. For p-$H_2$, only even rotational quantum numbers $j$ are allowed ($j = 0, 2, \ldots$), while o-$H_2$ can have exclusively odd rotational quantum numbers $j = 1, 3, \ldots$. In the absence of a catalyst, the introversion between the two nuclear spin isomers is extremely slow, which means that p-$H_2$ and o-$H_2$ behave as distinct physical species inside $C_{60}$.

$H_2@C_{60}$ constitutes an extraordinary nanoscale laboratory for both theoretical and experimental investigations of the intriguing quantum dynamical issues arising from the encapsulation of a light molecule in very confined spaces of high symmetry. Our fully coupled quantum five-dimensional (5D) calculations of the TR eigenstates of $H_2$ in $C_{60}$,[2,4,5] where the $H_2$ bond length is held fixed and $C_{60}$ is taken to be rigid, have resulted in the quantitative characterization of, and deep insight in, the "rattling" dynamics of the endohedral hydrogen. The most prominent, and unanticipated, feature of the TR dynamics of $H_2@C_{60}$ revealed already by our early studies[4] is the strong coupling between the orbital angular momentum

a)Electronic mail: zlatko.bacic@nyu.edu

 

associated with the translational motions of $H_2$ and the rotational angular momentum of the molecule. This TR coupling manifests conspicuously throughout the entire TR energy level structure, partially lifting the degeneracies of, and splitting the TR eigenstates of $H_2@C_{60}$ with simultaneous translational and rotational excitation.[2,4,5] Shortly thereafter, the first infrared (IR) spectra measured for $H_2@C_{60}$[6] showed absorption lines split into distinct peaks due to the TR coupling, as predicted by our calculations.[4,5] Subsequent IR spectroscopic studies of $H_2@C_{60}$,[3] as well as of endohedral HD and $D_2$ in $C_{60}$,[7] have provided a great deal of valuable information about the TR energy levels of the guest molecules and their interaction potentials with $C_{60}$. The physical properties of hydrogen endofullerens have also been probed by nuclear magnetic resonance (NMR).[1,8,9] What has enabled the experimental investigations is the synthetic organic breakthrough, known as "molecular surgery," by Komatsu and coworkers[10,11] for producing macroscopic amounts of $H_2@C_{60}$.

A powerful and versatile tool for elucidating with atomic-level resolution the behavior of molecular hydrogen entrapped in a variety of nanoscale cavities is the inelastic neutron spectroscopy (INS).[12,13] It owes its power and broad applicability to two unique features. One of them is the exceptionally large cross section for the incoherent neutron scattering from the hydrogen ($^1$H) nucleus,[14] ~15 times greater than for any other nucleus, including the isotope deuterium ($^2$H). This makes INS a highly selective probe of the dynamics of entrapped $H_2$ and HD molecules. The second distinctive feature of the INS is the ability of neutrons to change the total nuclear spin $I$ of the hydrogen molecule, something that photons cannot do. As a result, rotational $\Delta j = 1$ transitions can be observed, such as $j = 0 \rightarrow 1$ of p-$H_2$ ($I = 0$), and $j = 1 \rightarrow 0$ and $j = 1 \rightarrow 2$ of o-$H_2$ ($I = 1$), which interconvert p-$H_2$ and o-$H_2$; they are forbidden in the optical, IR and Raman spectroscopy. The rich information content of the INS spectra regarding the quantum TR dynamics of the caged guest molecule and its interaction with the host has been greatly underutilized for a long time, since only a small fraction of it could be reliably decoded by the low-dimensional, decoupled theoretical treatments employed in the analysis.[15–18]

Horsewill and co-workers have pioneered the use of INS in order to probe the quantum dynamics of $H_2$ and HD inside an open-cage fullerene[19] and in $C_{60}$.[20,21] They have recorded the INS spectra of $H_2@C_{60}$ for a range of the incident neutron wavelengths and at sample temperatures of 1.5, 120, and 240 K.[21] The peaks in the spectra correspond either to the transitions in which the neutrons transfer a part of their energy to the excitations of $H_2@C_{60}$, referred to as neutron energy (NE) loss, or the transitions where the $H_2$ molecules in excited TR eigenstates give up some of their energy to the scattered neutrons, referred to as NE gain. These investigations have led to the determination of the energies of the majority of the lower-lying TR eigenstates of $H_2@C_{60}$.[21] The interpretation and the assignment of the experimental INS spectra[20,21] have relied on the TR energy level structure of $H_2@C_{60}$ developed by us, in particular the TR coupling scheme.[2,4,5] Still, due to the limited spectrometer resolution, the bands associated with the multiplets arising from the TR coupling have largely not been resolved.[21]

The analysis and assignment of the experimental INS spectra of $H_2@C_{60}$, and nanoconfined molecules in general, would be more complete and reliable if in addition to accurate TR excitation energies, the theory could yield also the intensities of the INS transitions. It would then generate the complete spectroscopic fingerprint of the system considered for direct comparison with the experimental INS data. Recently, we have developed the quantum methodology which enables rigorous quantum simulation of the INS spectra of the hydrogen molecule confined inside a nanoscale cavity with an arbitrary shape.[22–24] What sets our approach apart from all other treatments in the literature is the incorporation of the coupled quantum 5D TR wave functions of the entrapped hydrogen molecule as the spatial parts of the initial and final states of the INS transitions.[22,23] This results in the simulated INS spectra which are exceptionally detailed and accurate,[22] and for the first time reflect in full the complexity of the TR dynamics of the guest molecule in nanoconfinement.

In this paper, we report the rigorous quantum calculations of the INS spectra of $H_2@C_{60}$, which simulate the experimental spectra and their temperature dependence[21] with high degree of realism and accuracy. Accurately calculated TR energy levels and INS transition intensities make it possible to assign with confidence the features present in the spectra recorded at several temperatures, removing the ambiguities about their interpretation. In particular, the origins of the broad structured feature in the NE gain spectrum of $H_2@C_{60}$ at 240 K,[21] for the incident neutron wavelength $\lambda_n = 5$ Å, are revealed; this prominent feature has not been analyzed previously because of its complexity. Our calculations show that most of the peaks comprising this feature are not due to a single dominant transition, but arise from two or more energetically close transitions with comparable intensities, originating in excited TR eigenstates. The matter is complicated further by the presence of other much weaker transitions in the same energy range. In this situation, typical for higher temperature INS spectra, the interpretation and assignment of the observed peaks is practically impossible without accurately calculated transition intensities. The results presented here signal that theory has reached a high level of sophistication and has matured to the point where it has considerable predictive power.

The other main result reported in this paper is the derivation of a new selection rule for INS, in Sec. III C and Appendix A, due to which the transitions between certain pairs of TR eigenstates of $H_2$ inside $C_{60}$ are strictly forbidden. Our calculations of the INS spectra confirm that these transitions, predicted to be forbidden, indeed have zero intensity. The existence of a selection rule in the INS spectroscopy of $H_2@C_{60}$ comes as a total surprise, as it runs counter to the widely held view that INS is not subject to any selection rules.[12,13]

## II. THEORY

### A. Calculation of the coupled 5D TR eigenstates of $H_2@C_{60}$

The methodology for the rigorous calculation of the 5D TR energy levels and wave functions of a hydrogen molecule inside fullerenes, applied in this work to $H_2@C_{60}$, has evolved

in our group over a number of years, in the course of the theoretical investigations of the quantum TR dynamics of $H_2$ and its isotopologues entrapped in the cages of clathrate hydrates,[25–27] fullerenes $C_{60}$, and $C_{70}$,[2,4] and an open-cage derivative of $C_{60}$ (ATOCF).[28] Since the detailed description of the quantum 5D methodology is available in Ref. 23, only the salient features are given here.

$C_{60}$ is treated as rigid, and its geometry used in our calculations has been determined experimentally, from the gas-phase electron diffraction study.[29] The bond length of $H_2$ is held fixed. This is justified by the fact that the intramolecular stretch frequency of $H_2$, ~4100 $cm^{-1}$, is much higher than those of the intermolecular TR modes. Therefore, the $H_2$ stretch vibration is coupled very weakly to the TR motions, and can be treated as frozen. The TR motions of $H_2$ inside the $C_{60}$ cage are described by the set of five coordinates ($x$, $y$, $z$, $\theta$, $\phi$); $x$, $y$, and $z$ are the Cartesian coordinates of the cm of $H_2$, while the two polar angles $\theta$ and $\phi$ specify its orientation relative to the cage. The origin of the Cartesian coordinate system is at the cm of the cage. The three rotational constants of $C_{60}$, a spherical top, are very small and equal to $2.803 \times 10^{-3}$ $cm^{-1}$, which justifies treating the fullerene as nonrotating. In this case, the 5D Hamiltonian for the TR motions of the caged diatomic molecule is[25]

$$H = -\frac{\hbar^2}{2\mu}\left(\frac{\partial^2}{\partial x^2} + \frac{\partial^2}{\partial y^2} + \frac{\partial^2}{\partial z^2}\right) + B\mathbf{j}^2 + V(x, y, z, \theta, \phi). \tag{1}$$

In Eq. (1), $\mu$ is the reduced mass of $H_2$ in $C_{60}$, and $\mathbf{j}^2$ is the angular momentum operator of the diatomic. $B$ denotes the rotational constant of the endohedral $H_2$ and will be discussed shortly. $V(x, y, z, \theta, \phi)$ in Eq. (1) is the 5D intermolecular potential energy surface (PES) for the interaction between the entrapped $H_2$ and the interior of $C_{60}$, which is described below. The TR energy levels and wave functions of the Hamiltonian in Eq. (1) are obtained utilizing the efficient computational methodology which originated in our group.[25,30] The final Hamiltonian matrix, its size drastically reduced by the sequential diagonalization and truncation procedure,[31] is diagonalized yielding the TR eigenstates which are numerically exact for the 5D PES employed. They are subsequently utilized in the computation of the INS spectra of $H_2$ in $C_{60}$, as outlined below.

Table I gives the parameters $B_e$, $\alpha_e$, and the centrifugal distortion parameter $D_e$, used in our quantum 5D calculations of the TR eigenstates; they have been extracted from the IR spectra of $H_2@C_{60}$.[3] The INS measurements probe the TR dynamics of $H_2$ in its ground intramolecular vibrational state ($v = 0$). Consequently, given that $B_v = B_e - \alpha_e(v + 1/2)$, the value of $B$ in Eq. (1) employed in the calculations is $B_0 = 58.378$ $cm^{-1}$. The reduced mass of $H_2@C_{60}$, 2.0104 amu, is only 0.3% smaller than the mass of $H_2$ molecule.

In the bound-state calculations,[23] the dimension of the sinc-discrete variable representation (DVR) basis was 15 for each of the three Cartesian coordinates $x$, $y$, and $z$, spanning the range $-2.83$ bohrs $\leq \lambda \leq 2.83$ bohrs ($\lambda = x, y, z$). For p-$H_2$, the angular basis included even-$j$ rotational functions up to $j_{max} = 6$, while the angular basis for o-$H_2$ included odd-$j$ rotational functions up to $j_{max} = 7$. The cutoff parameter for the size of the intermediate 3D eigenvector basis was set to 800 lowest-energy eigenvectors, resulting in the final 5D Hamiltonian matrices of dimension 22 400 for p-$H_2$ and 28 800 for o-$H_2$. These basis set parameters were chosen following extensive testing, assuring that the TR energy levels reported in this paper are converged to at least five significant figures.

TABLE I. Computational parameters used in this work. $\epsilon$ (in $cm^{-1}$) and $\sigma$ (in angstrom) are the LJ parameters in Eq. (7), and $\omega$ in Eq. (6) is dimensionless. They define the 5D intermolecular PES of $H_2@C_{60}$ and have been optimized by fitting the computed TR energy levels to the IR spectroscopic measurements for $H_2@C_{60}$ (Ref. 7). $B_e$ (equilibrium rotational constant), $\alpha_e$ (vibration-rotation constant), and $D_e$ (centrifugal distortion constant), all in $cm^{-1}$, for $H_2$ ($v = 0$) in $C_{60}$ are taken from Ref. 7.

| Parameter | Value |
|---|---|
| $\epsilon$(H–C) | 3.07 |
| $\sigma$(H–C) | 2.95 |
| $\omega$ | 6.7 |
| $B_e$ | 59.865 |
| $\alpha_e$ | 2.974 |
| $D_e$ | 0.04832 |

### B. Calculation of the INS spectra of $H_2@C_{60}$

The methodology for accurate quantum calculation of the INS spectra, both the energies and intensities of the transitions, of a hydrogen molecule confined inside a nanoscale cavity has been introduced recently.[22] It employs the 5D TR eigenstates of the Hamiltonian in Eq. (1) as the spatial components of the initial and final states of the INS transitions. For the case of the entrapped homonuclear molecule such as $H_2$, the details of the formalism are given in Ref. 23; its extension to the caged heteronuclear diatomics, e.g., HD, was presented in Ref. 24. For this reason, in the following we give only a few essential equations, define the key quantities, and elaborate on one important aspect of our quantum simulation of the INS spectra.

Let $E$ and $E'$ be the energies of the incident and scattered neutron, respectively, and $\vec{k}$ and $\vec{k}'$ their respective wave vectors. Then the neutron energy transfer can be written as $\hbar\omega = \Delta E = E - E'$, and the neutron momentum transfer as $\hbar\vec{\kappa} = \hbar\vec{k} - \hbar\vec{k}'$. The double differential cross section for neutron scattering in the first Born approximation is[32,33]

$$\frac{d^2\sigma}{d\Omega d\omega} = \frac{k'}{k} S(\vec{\kappa}, \omega), \tag{2}$$

where

$$S(\vec{\kappa}, \omega) = \sum_i p_i \sum_f \left|M_f^i\right|^2 \delta[\omega - (\epsilon_f - \epsilon_i)/\hbar] \tag{3}$$

and

$$M_f^i = \sum_n \langle f|\hat{b}_n \exp(i\vec{\kappa}\cdot\vec{r}_n)|i\rangle. \tag{4}$$

In Eqs. (2)–(4), $|i\rangle$ stands for the initial state of the scattering molecular system with the energy $\epsilon_i$, $p_i$ is its statistical weight, $|f\rangle$ is the final state with the energy $\epsilon_f$, $\hat{b}_n$ is the scattering

length operator (Ref. 23), and $\vec{r}_n$ is the position of nucleus $n$. In our case, the spatial components of $|i\rangle$ and $|f\rangle$ are different TR states of $H_2$ inside $C_{60}$, and are represented by the 5D TR eigenfunctions of the Hamiltonian in Eq. (1). The evaluation of $S(\vec{\kappa}, \omega)$ in Eq. (3) using the quantum 5D TR eigenstates is described in Ref. 23.

The experimental INS spectra of a hydrogen molecule in $C_{60}$ are taken from powdered samples,[20,21] where the fullerene cages are randomly oriented with respect to the incoming neutron beam. Therefore, in order to achieve a more realistic comparison with the measured spectra, the computed INS spectra are averaged over all possible orientations of $C_{60}$, as described previously.[23] Moreover, the IN4C spectrometer used by Horsewill and co-workers[21] allows the INS spectra of $H_2$ in $C_{60}$ to be recorded for a broad range of $\kappa \equiv |\vec{\kappa}|$ values. This means that $S(\kappa, \omega)$, obtained by averaging $S(\vec{\kappa}, \omega)$ in Eq. (3) over all directions of the wave vector $\vec{\kappa}$,[23] needs to be integrated also over $\kappa$ to obtain the desired $S(\omega)$. This is achieved by the procedure presented recently.[34]

The integration of the INS spectrum over both $\kappa$ and the angles $(\theta_{\vec{\kappa}}, \phi_{\vec{\kappa}})$ which define the direction of $\vec{\kappa}$ (to account for the random orientations of the $C_{60}$ cages) is performed for each distinct INS transition in the range of excitation energies considered. There were 1715 such transitions at the incident neutron wavelength $\lambda_n = 1.1$ Å and 587 INS transitions at $\lambda_n = 5.0$ Å. This procedure is computationally very time consuming, but it is worthwhile since it results in a realistic simulation of the experimental INS spectra. The integration over $\kappa$ was performed using the 20-point Gauss-Legendre quadrature. The numerical integration involved in the powder averaging was done using the 10-point Gauss-Legendre quadrature in $\theta_{\vec{\kappa}}$ and the 20-point Gauss-Chebyshev quadrature in $\phi_{\vec{\kappa}}$. This corresponds to a uniform $(\theta_{\vec{\kappa}}, \phi_{\vec{\kappa}})$ mesh on the surface of a sphere.

### C. Potential energy surface

As in all our previous theoretical studies of a hydrogen molecule inside fullerenes, the 5D intermolecular PES $V_{H_2-C_{60}}$ between the confined $H_2$ molecule and the carbon atoms of $C_{60}$ is assumed to be pairwise additive

$$V_{H_2-C_{60}}(\mathbf{q}) = \sum_{k=1}^{60} V_{H_2-C}(\mathbf{q}, \Xi_k), \tag{5}$$

where $\mathbf{q}$ are the coordinates $(x, y, z, \theta, \phi)$ of the endohedral $H_2$ defined above, $V_{H_2-C}$ is the pair interaction between $H_2$ and a carbon atom of the fullerene, and the index $k$ runs over all C atoms, whose coordinates $\Xi_k$ are fixed. $V_{H_2-C}$ is represented by the three-site pair potential[2]

$$V_{H_2-C}(\mathbf{q}, \Xi_k) = V_{LJ}(r_1) + V_{LJ}(r_2) + w V_{LJ}(r_m). \tag{6}$$

Here, $r_1$ and $r_2$ are the distances of the two H atoms of $H_2$ from the $k$th C atom of the fullerene, $r_m$ is the distance between the midpoint of the H–H bond and the $k$th C atom, while $w$ is a weight factor which allows us to effectively change the "shape" of $H_2$ seen by the $C_{60}$ interior, and thereby the angular anisotropy of the interaction potential between the two entities.[2] $V_{LJ}(r)$ in Eq. (6) is the standard Lennard-Jones (LJ) 12-6 potential given by

$$V_{LJ}(r) = 4\epsilon_{HC}\left[\left(\frac{\sigma_{HC}}{r}\right)^{12} - \left(\frac{\sigma_{HC}}{r}\right)^{6}\right], \tag{7}$$

where $\epsilon_{HC}$ is the well depth of the potential and $\sigma_{HC}$ is related to its equilibrium distance $r_e$, as $r_e = 2^{1/6}\sigma_{HC}$. The LJ parameters $\epsilon$(H–C) and $\sigma$(H–C), as well as the weight factor $\omega$,[2] are listed in Table I. They were determined by achieving the best match between the calculated TR energy levels of $H_2$ ($v = 0$) in $C_{60}$ and those obtained by fitting the IR spectroscopic data[3] for this system.

## III. RESULTS AND DISCUSSION

### A. Quantum numbers and the TR energy level diagram of $H_2$@$C_{60}$

It has been established previously[4] that the rigorously computed quantum 5D TR energy level structure of $H_2$@$C_{60}$ can be organized and assigned relying on the following model: (i) The 3D isotropic harmonic oscillator (HO) is used to classify the purely translational eigenstates of $H_2$ (although they exhibit pronounced negative anharmonicity). They are assigned with the principal quantum number $n = 0, 1, 2, \ldots$, of the 3D HO and its orbital angular momentum quantum number $l = n, n-2, \ldots, 1$ or 0, for odd and even $n$, respectively. (ii) The quantum number $j = 0, 1, 2, \ldots$, of the rigid rotor is used for assigning the purely rotational energy levels of the caged $H_2$. (iii) In the case of the TR eigenstates which are excited *both* translationally and rotationally, the orbital angular momentum $\boldsymbol{l}$ and the rotational angular momentum $\boldsymbol{j}$ *couple* vectorially to give the total angular momentum $\boldsymbol{\lambda} = \mathbf{l} + \mathbf{j}$ having the values $\lambda = l + j, l + j - 1, \ldots, |l - j|$, and the degeneracy of $2\lambda + 1$. The values of $l$ are those allowed for the quantum number $n$. The eigenstates with the same quantum numbers $n$ and $j$ (both nonzero) are *split*, due to the TR coupling, into as many distinct levels as there are different values of $\lambda$, each having the degeneracy of $2\lambda + 1$.[4]

The predicted splitting of the (nine) $n = l = 1$, $j = 1$ eigenstates into three levels corresponding, in ascending order, to $\lambda = 1$, 2, and 0,[4] was later observed in both the IR[6] and INS spectra[21] of $H_2$@$C_{60}$, that validating the concept of the TR coupling and its spectroscopic manifestations.

The lower-lying TR energy levels of $H_2$@$C_{60}$, from the quantum 5D calculations for $H_2$ in the ground vibrational state $v = 0$, are shown in Fig. 1; they are assigned with the quantum numbers $n, j, \lambda, l$. The energy levels in the first and last columns are those of p-$H_2$ for $j = 0$ and 2, respectively, while the levels in the middle column ($j = 1$) belong to o-$H_2$. The ground state (0, 1, 1, 0) of o-$H_2$ lies 14.5 meV above the ground state (0, 0, 0, 0) of p-$H_2$.

### B. Low-temperature INS spectra of $H_2$@$C_{60}$

The INS spectra for the incident neutron wavelength $\lambda_n = 1.1$ Å used in the experiments, computed for 0 K and recorded at 1.6 K[21] are shown in Fig. 2. The simulations are performed for the statistical 3:1 mixture of o-$H_2$ and p-$H_2$, expected for the room temperature (or higher) at which $H_2$@$C_{60}$

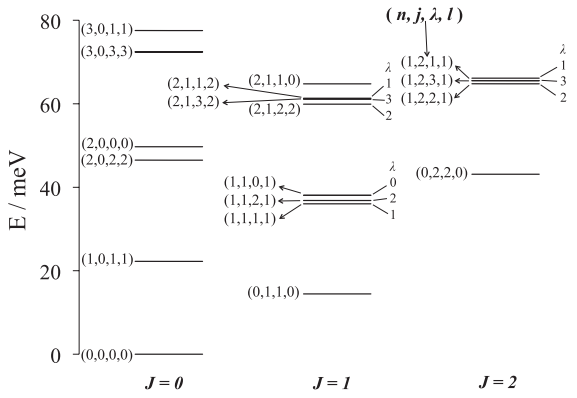


FIG. 1. Lower-lying translation-rotation (TR) energy levels of p-$H_2$ and o-$H_2$ molecule inside $C_{60}$ from the quantum 5D calculations. They are labeled by the quantum numbers ($n$, $j$, $\lambda$, $l$) defined in the text, and are arranged in columns according to their $j$ values. Most of these energy levels were observed in the measured INS spectra of $H_2$@$C_{60}$ in Ref. 21. This includes the $n = 1$, $j = 1$ triplet, the fundamental translational excitation of o-$H_2$, whose splitting into the components with the total angular momentum values $\lambda = 1$, 2, and 0, respectively, due to the TR coupling was predicted by theory (Ref. 4).

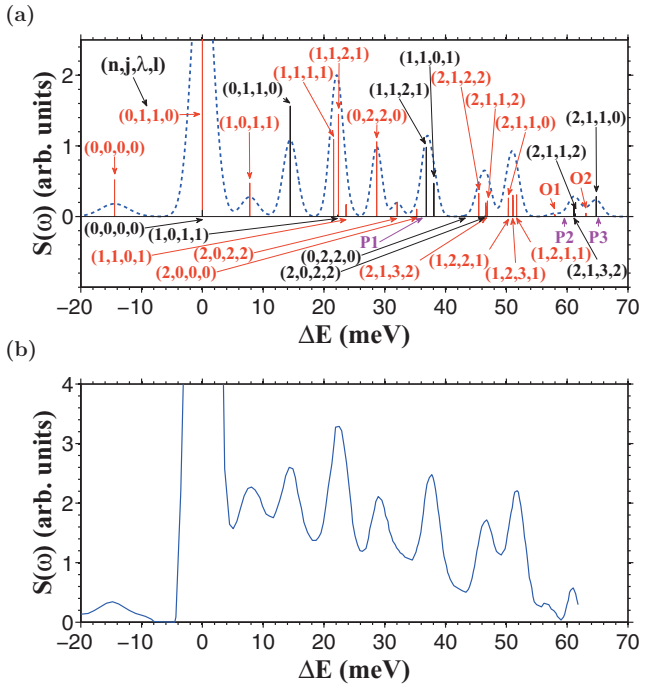


FIG. 2. Calculated and measured low-temperature INS spectra of $H_2$@$C_{60}$, for the incident neutron wavelength $\lambda_n = 1.1$ Å. (a) The INS spectrum computed for 0 K, assuming 3:1 ratio of o-$H_2$ to p-$H_2$. The quantity on the horizontal axis is the neutron energy transfer $\Delta E = E - E'$, where $E$ and $E'$ are the energies of the incident and scattered neutron, respectively. $\Delta E$ is positive in NE loss and negative in NE gain. The stick spectra are convolved with the instrumental resolution function. The transitions originating in the ground state of p-$H_2$ are shown with black vertical lines and the quantum numbers of their final states are in black, while the transitions from the ground state of o-$H_2$ are represented with red vertical lines and the quantum numbers of their final states are in red. For greater clarity, several transitions are labeled with letter symbols: O1 (0,1,1,0) → (3,0,3,3) and O2 (0,1,1,0) → (3,0,1,1). The energies of the three transitions which are forbidden by the selection rule described in the text are indicated as P1 (0,0,0,0) → (1,1,1,1), P2 (0,0,0,0) → (2,1,2,2), and P3 (0,0,0,0) → (1,2,2,1). (b) The experimental INS spectrum recorded at 1.6 K, from Fig. 6 (top) in Ref. 21.

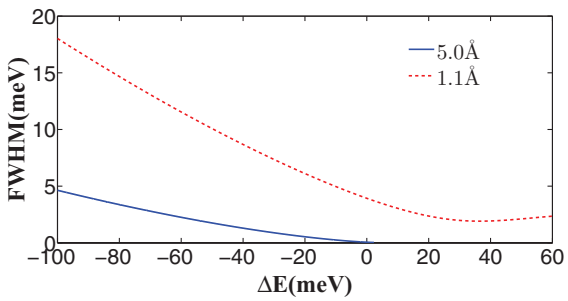


FIG. 3. The full widths at half maximum (FWHM) of the standard Gaussian functions as a function of the neutron energy transfer $\Delta E$, for two incident neutron wavelengths $\lambda_n$, 1.1, and 5.0 Å. They represent the experimental resolution functions.

is prepared.[1] Subsequent cooling of the sample in absence of an external catalyst does not alter this equilibrium ratio. The calculated stick spectra are convolved with the appropriate instrumental resolution function defined in Fig. 3. At 1.6 K, the INS transitions, calculated or observed, must originate exclusively in ground TR states of either p-$H_2$ (0, 0, 0, 0) or o-$H_2$ (0, 1, 1, 0), since they are the only ones populated at this low temperature. Therefore, with one exception discussed below, all the transitions appear in NE loss. The computed energies and intensities of the INS transitions present in Fig. 2(a), out of the ground TR states of p-$H_2$ and o-$H_2$, are given in Tables II and III, respectively.

A glance at Fig. 2 reveals a virtually perfect match between the calculated and measured INS spectra; they are in excellent agreement with respect to both the positions and relative intensities of the peaks shown. This enables unambiguous interpretation of the experimental spectrum. All the peaks

TABLE II. Calculated intensities of the INS transitions out of the ground state (0, 0, 0, 0) of p-$H_2$@$C_{60}$, for the incident neutron wavelength $\lambda_n = 1.1$ Å, in the units of barn (bn); 1 barn = $1 \times 10^{-24}$ $cm^2$. $\Delta E$ is the neutron energy transfer. For the final states of the transitions, listed are their degeneracies $g$ and the quantum numbers explained in the text. The bold-faced transitions are forbidden according to the selection rule derived in this paper.

| $\Delta E$ ($cm^{-1}$) | $\Delta E$ (meV) | Intensity (bn) | $g$ | ($n$, $j$, $\lambda$, $l$) | $j \rightarrow j$ |
|---|---|---|---|---|---|
| 0.00 | 0.000 | 18.088 | 1 | (0,0,0,0) | 0→0 |
| 116.53 | 14.448 | 312.924 | 3 | (0,1,1,0) | 0→1 |
| 179.39 | 22.242 | 4.560 | 3 | (1,0,1,1) | 0→0 |
| 290.63 | 36.033 | **0.000** | 3 | **(1,1,1,1)** | 0→1 |
| 297.02 | 36.826 | 196.376 | 5 | (1,1,2,1) | 0→1 |
| 307.14 | 38.080 | 94.296 | 1 | (1,1,0,1) | 0→1 |
| 347.80 | 43.121 | 1.216 | 5 | (0,2,2,0) | 0→2 |
| 374.95 | 46.487 | 1.339 | 5 | (2,0,2,2) | 0→0 |
| 400.93 | 49.709 | 0.439 | 1 | (2,0,0,0) | 0→0 |
| 483.20 | 59.908 | **0.000** | 5 | **(2,1,2,2)** | 0→1 |
| 492.65 | 61.080 | 35.801 | 4 | (2,1,3,2) | 0→1 |
| 493.16 | 61.144 | 26.775 | 3 | (2,1,3,2) | 0→1 |
| 494.66 | 61.329 | 8.326 | 3 | (2,1,1,2) | 0→1 |
| 522.48 | 64.778 | 56.733 | 3 | (2,1,1,0) | 0→1 |
| 522.56 | 64.788 | **0.000** | 5 | **(1,2,2,1)** | 0→2 |
| 528.49 | 65.524 | 0.357 | 4 | (1,2,3,1) | 0→2 |
| 528.55 | 65.531 | 0.265 | 3 | (1,2,3,1) | 0→2 |
| 533.45 | 66.139 | 0.356 | 3 | (1,2,1,1) | 0→2 |

TABLE III. Calculated intensities of the INS transitions out of the ground state (0, 1, 1, 0) of o-$H_2$@$C_{60}$, for the incident neutron wavelength $\lambda_n = 1.1$ Å, in the units of barn (bn); 1 barn $= 1 \times 10^{-24}$ cm$^2$. $\Delta E$ is the neutron energy transfer. For the final states of the transitions, listed are their degeneracies $g$ and the quantum numbers explained in the text.

| $\Delta E$ (cm$^{-1}$) | $\Delta E$ (meV) | Intensity (bn) | $g$ | $(n, j, \lambda, l)$ | $j \rightarrow j$ |
|---|---|---|---|---|---|
| − 116.53 | −14.448 | 34.813 | 1 | (0,0,0,0) | 1→0 |
| 0.00 | 0.000 | 588.476 | 3 | (0,1,1,0) | 1→1 |
| 62.86 | 7.794 | 31.702 | 3 | (1,0,1,1) | 1→0 |
| 174.10 | 21.585 | 72.955 | 3 | (1,1,1,1) | 1→1 |
| 180.49 | 22.378 | 96.433 | 5 | (1,1,2,1) | 1→1 |
| 190.61 | 23.633 | 11.484 | 1 | (1,1,0,1) | 1→1 |
| 231.27 | 28.674 | 70.712 | 5 | (0,2,2,0) | 1→2 |
| 258.42 | 32.039 | 13.451 | 5 | (2,0,2,2) | 1→0 |
| 284.40 | 35.261 | 7.029 | 1 | (2,0,0,0) | 1→0 |
| 366.67 | 45.461 | 21.945 | 5 | (2,1,2,2) | 1→1 |
| 376.12 | 46.632 | 13.104 | 4 | (2,1,3,2) | 1→1 |
| 376.63 | 46.696 | 9.808 | 3 | (2,1,3,2) | 1→1 |
| 378.13 | 46.881 | 14.836 | 3 | (2,1,1,2) | 1→1 |
| 405.94 | 50.330 | 17.521 | 3 | (2,1,1,0) | 1→1 |
| 406.03 | 50.340 | 8.482 | 5 | (1,2,2,1) | 1→2 |
| 411.96 | 51.076 | 20.264 | 4 | (1,2,3,1) | 1→2 |
| 412.02 | 51.083 | 15.171 | 3 | (1,2,3,1) | 1→2 |
| 416.92 | 51.691 | 20.669 | 3 | (1,2,1,1) | 1→2 |
| 467.25 | 57.932 | 2.041 | 4 | (3,0,3,3) | 1→0 |
| 468.12 | 58.039 | 1.519 | 3 | (3,0,3,3) | 1→0 |
| 508.89 | 63.094 | 3.060 | 3 | (3,0,1,1) | 1→0 |

are assigned, and the energies mentioned are for the computed spectra.

The only peak present in NE gain at this temperature, at −14.4 meV, arises from the transition (0, 1, 1, 0) → (0, 0, 0, 0) which interconverts o-$H_2$ and p-$H_2$ in their ground TR states. This peak exists due to the inability of the two spin isomers of $H_2$ to interconvert spontaneously as the sample temperature is lowered, so that their relative populations are frozen at the values when the sample was prepared.[21] The reverse of this transition gives rise to the NE loss peak at 14.4 meV.

The peak at 7.8 meV is due to another transition connecting the o-$H_2$ and p-$H_2$ manifolds, this time between the ground TR state (0, 1, 1, 0) of o-$H_2$ to the translational fundamental (1, 0, 1, 1) of p-$H_2$. Horsewill *et al.*[21] have made the same assignment by considering the TR energy level diagram for $H_2$@$C_{60}$ similar to the one shown in Fig. 1.

Of particular interest is the prominent band at 22 meV which has received close experimental scrutiny,[20,21] since it is the first to demonstrate the effects of TR coupling. It is associated with the transition from the ground TR state (0, 1, 1, 0) of o-$H_2$ to its first excited translational state, which consists of three (1, 1, λ, 1) sublevels with the total angular momentum quantum number λ = 1, 2, 0, respectively, split unevenly by the TR coupling[2,4] (Fig. 1). In the computed stick spectrum in Fig. 2(a), this band appears as a strongly asymmetric triplet of transitions (0, 1, 1, 0) → (1, 1, λ, 1), λ = 1, 2, 0. The intensities of the λ = 1 and λ = 2 components are comparable, while the intensity of the λ = 0 member is much weaker, by nearly a factor of ten (see Table III). The splitting of the triplet components is unequal as well; the splitting between the λ = 0 and λ = 2 components is significantly larger than that between the λ = 1 and λ = 2 components. The experimental INS spectra[20,21] have not yet fully resolved this triplet structure. In their more recent study, Horsewill *et al.*[21] have revisited the 22 meV band and recorded it with greater sensitivity and resolution, and lower background. Then, guided by our theoretical predictions,[2,4] they have fitted this band to a triplet of Gaussians, and extracted the energies and the amplitudes of the three transitions. The λ = 0 component, barely a shoulder in the spectrum, has the amplitude that is much smaller than the λ = 1, 2 amplitudes; the latter have similar magnitudes.[21] Moreover, the separation between the λ = 0 and λ = 2 components is considerably greater than the splitting of the λ = 1 and λ = 2 members. The agreement between the calculated and the measured splittings, both the total for the triplet and between the individual λ components, is near-quantitative.

The peak centered at 28.7 meV corresponds to the purely rotational transition (0, 1, 1, 0) → (0, 2, 2, 0) between o-$H_2$ and p-$H_2$.

A small peak at 32 meV is associated with the (0, 1, 1, 0) → (2, 0, 2, 2) transition between o-$H_2$ and p-$H_2$. The closely related o-$H_2$–p-$H_2$ transition (0, 1, 1, 0) → (2, 0, 0, 0) to the $l = 0$ component of the upper state at 35.3 meV lies within the band at 37 meV. It also has a relatively small intensity, and therefore Horsewill *et al.*[21] were unable to find any evidence for it in the spectrum.[21] We will return to the 37 meV band for a closer look shortly, since it hides one of the most significant findings of this paper – existence of forbidden INS transitions.

The band at 46 meV is quite complex. It arises from the two-quanta translational excitation of o-$H_2$, from its ground TR state (0, 1, 1, 0) to what is the $n = 2$, $j = 1$ multiplet. This multiplet consists of three $l = 2$ states which are, in ascending energy, (2, 1, λ, 2), with λ = 2, 3, 1, and one $l = 0$ state (2, 1, 1, 0) about 3.5 meV higher in energy (see Fig. 1 and Table III); the fact that the energies of the translationally excited states depend not only on $n$ but also on $l$ is evidence of their anharmonicity.[4] Fig. 2(a) shows that 46 meV band is composed of the transitions to the three $l = 2$ states, which are split in an uneven fashion by the TR coupling. In the experimental INS spectrum[21] this band is not sufficiently resolved to reveal the triplet structure and the energies of the individual transitions, see Fig. 2(b).

The transition to the $l = 0$ component, (0, 1, 1, 0) → (2, 1, 1, 0), is calculated to be at 50.3 meV. As evident from Fig. 2(a), this places it within the experimentally unresolved band at 52 meV, together with the TR coupling split triplet (0, 1, 1, 0) → (1, 2, λ, 1), λ = 2, 3, 1. For this reason, the (0, 1, 1, 0) → (2, 1, 1, 0) transition has not been identified in the INS spectrum,[21] although its intensity is comparable with that of the other near-by transitions.

The INS spectrum for $\Delta E \geq 60$ meV illustrates the challenges of assigning the peaks in the higher energy regions of the spectrum in which the density of the TR energy levels increases rapidly. Tables II and III show the following eight transitions with $\Delta E$ between 60 and 66 meV: out of p-$H_2$ (0, 0, 0, 0) → (2, 1, λ, 2) with λ = 2, 3, 1 and (0, 0, 0, 0) → (2, 1, 1, 0), (0, 0, 0, 0) → (1, 2, λ, 1) with λ = 2, 3, 1; out of o-$H_2$ (0, 1, 1, 0) → (3, 0, 1, 1). But, just two of these transitions have significant intensities, (0, 0, 0, 0) → (2, 1, 3,

2) and (0, 0, 0, 0) → (2, 1, 1, 0), and give rise to the two bands at 61 and 65 meV in the computed INS spectrum in Fig. 2(a). Minor contributions come from the very weak transitions (0, 0, 0, 0) → (2, 1, 1, 2) and (0, 1, 1, 0) → (3, 0, 1, 1).

Clearly, without the information provided by theory about the intensities of the transitions, it would be virtually impossible to assign with confidence the experimental INS spectrum for these and higher excitation energies and extract reliable TR energy levels. The following example is instructive. In Table II of Ref. 21 the band at 66.5 meV is assigned to the (1, 2, λ, 1) λ = 2, 3, 1 triplet solely on energetic considerations. While reasonable, this assignment is incorrect, since all transitions (0, 0, 0, 0) → (1, 2, λ, 1) with λ = 2, 3, 1 have negligible intensities, as evident from Table II, and therefore do not appear in the INS spectrum at all. As discussed in the preceding paragraph, this band is due to the moderately intense (0, 0, 0, 0) → (2, 1, 1, 0) transition in the same energy range.

We now return to the band at 37 meV. It is composed of the transitions from the ground TR state of p-$H_2$ to the $n = 1, j = 1$ triplet of o-$H_2$, which consists of three (1, 1, λ, 1) levels having the total angular momentum quantum numbers λ = 1, 2, 0, respectively (see Fig. 1). Therefore, *three* transitions should be present in the calculated spectrum, corresponding to (0, 0, 0, 0) → (1, 1, λ, 1), λ = 1, 2, 0. However, *only two* transitions are visible (Fig. 2(a)), with the λ = 2 and λ = 0 levels as the final states. The λ = 1 transition, with the calculated energy of 36.0 meV, is absent (in Fig. 2(a) its position is marked as P1), and it has *zero* intensity, see Table II. This is not accidental; the transition (0, 0, 0, 0) → (1, 1, 1, 1) is *strictly forbidden* according to the new *selection rule* which we formulate in Sec. III C. The absence of this transition in the INS spectrum of $H_2@C_{60}$ has not been detected experimentally yet,[21] partly due to the limited resolution of the measurements, and also because it is masked by the transitions (0, 1, 1, 0) → (2, 0, 0, 0) (weak) and (0, 0, 0, 0) → (1, 1, 2, 1) (strong), which are energetically close to the forbidden transition.

### C. Selection rule for the INS spectra

As pointed out in the Introduction, it has been largely taken for granted that the INS spectroscopy of molecular systems, including the supramolecular complex $H_2@C_{60}$, is free from any selection rules,[12,13] unlike the IR or Raman spectroscopy. The only exception found to date have been the phonon symmetry selection rules established for the INS by crystals,[35,36] based on the space group symmetry. Here we demonstrate that this widespread belief is not completely correct, by establishing the following INS selection rule:

*Consider the* p-$H_2$ *molecule confined in a near-spherical environment, such as that of* $C_{60}$, *where its orbital angular momentum* $\boldsymbol{l}$ *and the rotational angular momentum* $\boldsymbol{j}$ *couple to give the total angular momentum* $\boldsymbol{\lambda}$, *with the eigenvalues* $\lambda = l + j, l + j - 1, \ldots, |l - j|$. *Then the INS transition involving the ground state* (0, 0, 0, 0) *of* p-$H_2$ *and the excited state* (*n*, *j*, λ, *l*) is **forbidden** *for* $\boldsymbol{\lambda = j + l - 1}$, *in both NE loss and NE gain.*

The values of *l* are $n, n - 2, \ldots, 1$ or 0, for odd and even $n$, $n = 0, 1, 2\ldots$ being the principal quantum number of the 3D HO, while $j = 0, 1, 2, \ldots$ is the quantum number of the rigid rotor.

The starting point for the derivation of this selection rule is the spatial component of the INS transition matrix element[22,23]

$$I_f^i = \left\langle \Psi_f^{5D} \right| \exp(i\vec{\kappa} \cdot \vec{R}_{\rm cm}) \exp\left( i \frac{\vec{\kappa} \cdot \vec{\rho}}{2} \right) \left| \Psi_i^{5D} \right\rangle, \qquad (8)$$

where $|\Psi_i^{5D}\rangle$ and $|\Psi_f^{5D}\rangle$ are two different 5D eigenstates of the TR Hamiltonian in Eq. (1). They constitute the spatial parts of the $|i\rangle$ and $|f\rangle$ states of the INS transition, respectively, which appear in Eqs. (3) and (4). In Eq. (8), $\vec{R}_{\rm cm}$ is the position vector of the cm of $H_2$, $\vec{\rho}$ is the vector connecting the two H atoms, and $\vec{\kappa}$ is the wave vector of the neutron momentum transfer.[22,23] One needs to show that the matrix element $I_f^i$ in Eq. (8) between the TR states (0, 0, 0, 0) and (*n*, *j*, λ, *l*) is equal to zero when $\lambda = j + l - 1$. The proof is rather lengthy and is therefore presented in Appendix A.

The (0, 0, 0, 0) → (1, 1, 1, 1) transition, P1 in Fig. 2(a), is not the only one in NE loss which is forbidden by the above selection rule. Two other transitions, (0, 0, 0, 0) → (2, 1, 2, 2) at 59.9 meV and (0, 0, 0, 0) → (1, 2, 2, 1) at 64.8 meV, marked in Fig. 2(a) as P2 and P3, respectively, are forbidden as well. The calculated intensities of these two transitions are zero, as shown in Table II. Of course, each of these transitions in the reverse direction, which would lie in NE gain, is also forbidden.

### D. Temperature dependence of the INS spectra

The expression for the INS scattering cross section, Eqs. (2)–(4), involves summation over the initial states of the system weighted by their relative populations according to the Boltzmann distribution for the given temperature. Consequently, the INS spectra exhibit a strong temperature dependence. With increasing temperature, a growing number of excited TR states becomes appreciably populated, greatly increasing the number of transitions capable of giving rise to new peaks in the INS spectrum. In the NE gain, some of these new peaks represent reversals of the transitions already found in the NE loss at low temperature, but many more arise from previously unobserved transitions originating in higher lying TR eigenstates, and blend into broad bands. The makes the assignments very difficult and heavily reliant on theory, particularly the computed INS transition intensities. Figs. 4–6 display the calculated and measured[21] INS spectra of $H_2@C_{60}$ at 1.6, 120, and 240 K, with the incident neutron wavelength $\lambda_n = 5$ Å. The individual transitions are not shown in the calculated spectra to avoid congestion. The calculations assume the statistical 3:1 mixture of the entrapped o-$H_2$ and p-$H_2$. Fig. 4 gives the global view of the theoretical and measured INS spectra over the entire energy transfer range considered, $-56 \le \Delta E \le 4$ meV, while Figs. 5 and 6 show the spectra in more details, and with the quantum numbers assignments, for two more limited energy transfer regions.

Fig. 4 demonstrates an excellent overall agreement between the computed and measured temperature dependence

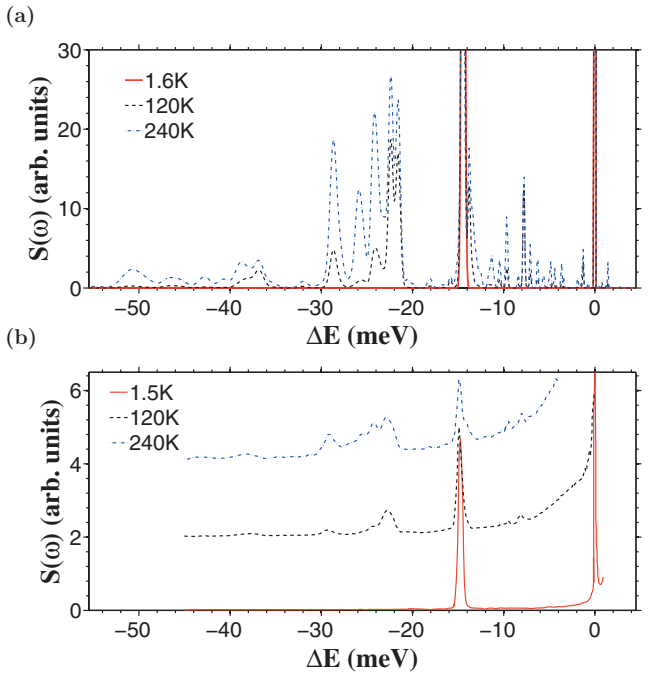


FIG. 4. Calculated and measured temperature dependence of the INS spectrum of $H_2@C_{60}$, in NE gain, for the incident neutron wavelength $\lambda_n = 5$ Å: I. An overview, from −56 to 4 meV. (a) The INS spectra computed for 1.6, 120, and 240 K, assuming 3:1 ratio of o-$H_2$ to p-$H_2$. The stick spectra are convolved with the instrumental resolution function. (b) The experimental INS spectra recorded at 1.5, 120, and 240 K, from Fig. 7 (top) in Ref. 21.

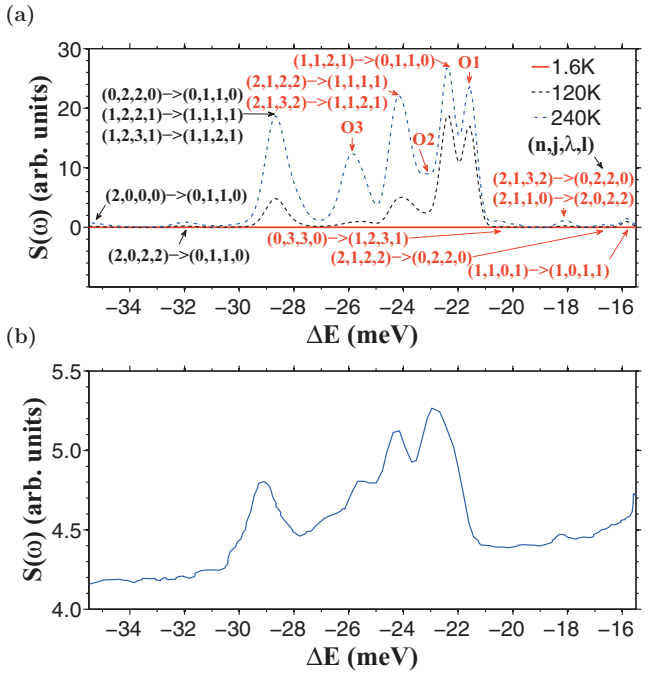


FIG. 5. Calculated and measured temperature dependence of the INS spectrum of $H_2@C_{60}$, in NE gain, for the incident neutron wavelength $\lambda_n = 5$ Å: II. A more detailed view, from −35.5 to −15.5 meV. (a) The INS spectra computed for 1.6, 120, and 240 K, assuming 3:1 ratio of o-$H_2$ to p-$H_2$. The stick spectra are convolved with the instrumental resolution function. For greater clarity, several transitions are labeled with letter symbols: O1 (1,1,1,1) → (0,1,1,0); O2 (1,1,0,1) → (0,1,1,0) and (2,1,1,2) → (1,1,0,1) and (2,1,2,2) → (1,1,2,1); O3 (3,1,3,3) → (2,1,2,2) and (3,1,4,3) → (2,1,3,2) and (3,1,2,3) → (2,1,1,2) and (2,1,1,0) → (1,1,1,1). (b) The experimental INS spectrum recorded at 240 K, taken from Fig. 7 (top) in Ref. 21.

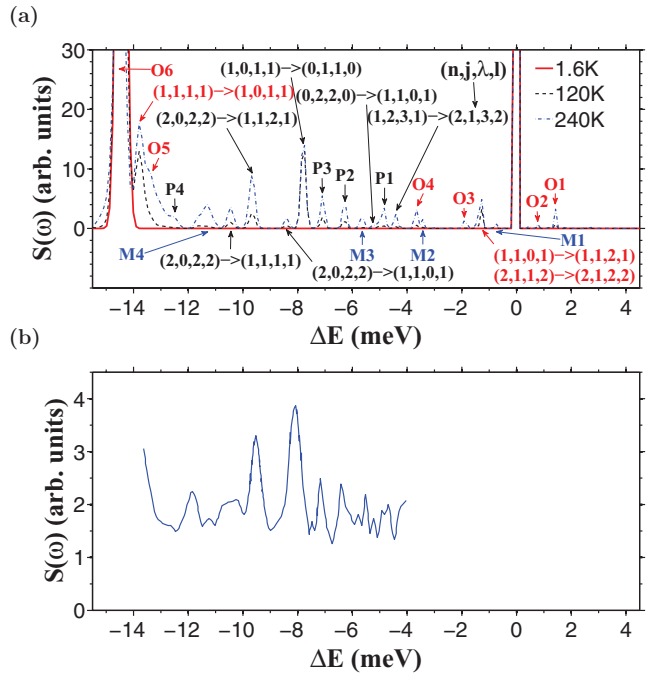


FIG. 6. Calculated and measured temperature dependence of the INS spectrum of $H_2@C_{60}$, mostly in NE gain, for the incident neutron wavelength $\lambda_n = 5$ Å: III. A more detailed view, from −15.5 to 4.0 meV. (a) The INS spectra computed for 1.6, 120, and 240 K, assuming 3:1 ratio of o-$H_2$ to p-$H_2$. The stick spectra are convolved with the instrumental resolution function. For greater clarity, many peaks are labeled with letter symbols O/P for transitions from the TR states of ortho/para-$H_2$, or M when the peak consists of transitions originating in the TR states of both ortho-$H_2$ and para-$H_2$: O1 (1,1,2,1) → (1,1,0,1) and (2,1,2,2) → (2,1,1,2); O2 (1,1,1,1) → (1,1,2,1) and (2,1,1,0) → (1,2,3,1); O3 (3,1,0,1) → (3,1,2,1) and (3,1,2,3) → (3,1,3,3); O4 (2,1,1,0) → (2,1,3,2); O5 (2,1,2,2) → (2,0,2,2) and (3,1,3,3) → (3,0,3,3); O6 (0,1,1,0) → (0,0,0,0) and (1,1,2,1) → (1,0,1,1) and (2,1,3,2) → (2,0,2,2); P1 (1,2,2,1) → (2,1,2,2) and (1,2,1,1) → (2,1,1,2); P2 (0,2,2,0) → (1,1,2,1); P3 (0,2,2,0) → (1,1,1,1); P4 (3,0,3,3) → (2,1,2,2) and (3,0,1,1) → (2,1,1,0) and (2,0,0,0) → (1,1,2,1); M1 (1,1,2,1) → (1,1,1,1) and (1,2,3,1) → (2,1,1,0); M2 (1,2,2,1) → (2,1,1,2) and (3,1,1,1) → (3,1,2,3) and (2,1,1,0) → (2,1,1,2); M3 (3,1,2,1) → (3,1,4,3) and (1,2,3,1) → (2,1,2,2); M4 (3,0,3,3) → (2,1,3,2) and (3,0,3,3) → (2,1,2,2) and (2,0,0,0) → (1,1,0,1) and (2,1,1,2) → (2,0,0,0). (b) The experimental INS spectrum recorded at 240 K, from −14 to −4 meV, taken from Fig. 7 (top) in Ref. 21.

of the INS spectra. The calculations reproduce correctly the peaks present in the measured spectra, their relative heights and temperature variations. First, we discuss the part of the spectrum in NE gain at energy transfers $|\Delta E| > 20$ meV, for 240 K, displayed in Fig. 5, which has not been analyzed previously.[21] The five main peaks in the calculated INS spectrum (Fig. 5(a)) between −20 and −30 meV correspond very well to the partially resolved structure on top of the broad feature of the measured spectrum in the same energy range (Fig. 5(b)). The two peaks around −22 meV are the NE gain partners of the band observed at 22 meV in NE loss at low temperature (Fig. 2), and correspond to the transitions from the first translationally excited state of o-$H_2$ to its ground TR state. The peak labelled O1 is due to the (1, 1, 1, 1) → (0, 1, 1, 0) transition at −21.58 meV, while the peak at −22.38 arises from the (1, 1, 2, 1) → (0, 1, 1, 0) transition. As in the NE loss, the third transition (1, 1, 0, 1) → (0, 1, 1, 0) at −23.63 meV, labelled O2, cannot be resolved individually, since it has a

much weaker intensity than the other two transitions, and also because it lies between two strong bands.

Two transitions make the dominant, and similar, contributions to the peak at −24 meV, (2, 1, 2, 2) → (1, 1, 1, 1) at −23.88 meV and (2, 1, 3, 2) → (1, 1, 2, 1) at −24.25 meV. Both represent the de-excitation of o-$H_2$ from the second to first excited translational states (Fig. 1). It should be pointed out that there are two other transitions between the energies of these dominant transitions, but their calculated intensities are negligible. In the absence of the information about the intensities, the assignment of this peak would not be feasible.

The peak labelled O3 in Fig. 5(a) at −26 meV illustrates even better the difficulties which the experimentalists encounter in trying to make assignments of the features far in the NE gain spectrum. Our calculations show that this peak arises from a number of transitions close in energy, all of which have small and comparable intensities: (2, 1, 1, 0) → (1, 1, 1, 1) at −25.30 meV, (3, 1, 3, 3) → (2, 1, 2, 2) at −25.64 meV, (3, 1, 4, 3) → (2, 1, 3, 2) at −25.98 meV, and (3, 1, 2, 3) → (2, 1, 1, 2) at −26.72 meV. To make the matters worse, in the same energy range numerous other transitions exist whose computed intensities are negligible.

The same holds for the last major peak in Fig. 5(a) at −28.7 meV, which is also a composite of several transitions. The strongest one is (0, 2, 2, 0) → (0, 1, 1, 0) at −28.67 meV, while smaller contributions come from (1, 2, 2, 1) → (1, 1, 2, 1) at −27.96 meV, (1, 2, 3, 1) → (1, 1, 2, 1) at −28.70 meV, and (1, 2, 2, 1) → (1, 1, 1, 1) at −28.76 meV. In addition, several much weaker transitions lie in the energy range spanned by the stronger ones.

Next, we briefly discuss the portion of the INS spectrum displayed in Fig. 6. Again, the agreement between the calculated and recorded spectra is remarkable. What is particularly interesting about this region of the spectrum is that many of its features are fingerprints of the (1, 1, λ, 1) $\lambda = 1, 2, 3$ triplet of o-$H_2$.

With increasing temperature, a strong peak emerges at −13.79 meV (Fig. 6(a)), which is associated with the transition from the $\lambda = 1$ component of the (1, 1, λ, 1) triplet of o-$H_2$ to the state (1, 0, 1, 1) of p-$H_2$ (see Fig. 1). The analogous transition originating in the $\lambda = 2$ member of the triplet, at −14.58 meV, overlaps completely with the dominant (0, 1, 1, 0) → (0, 0, 0, 0) transition at −14.45 meV (O6 in Fig. 6(a)) and cannot be resolved. The transition from the $\lambda = 0$ member of this triplet appears as a small peak at −15.84 meV in Fig. 5(a).

The peaks at −10.45, −9.66, and −8.41 meV in Fig. 6(a) arise from the transitions originating in the state (2, 0, 2, 2) of p-$H_2$ to the $\lambda = 1$, 2, and 0 members of the (1, 1, λ, 1) triplet of o-$H_2$, respectively. The counterparts of the first two computed transitions are clearly visible in the experimental spectrum at −10.25 and −9.53 meV, while the third overlaps with the more intense band peaking at −8.11 meV (see Fig. 6(b)).

The peaks at −7.09 (P3), −6.30 (P2), and the barely visible one at −5.04 meV (Fig. 6(a)), also involve transitions to the $\lambda = 1$, 2, and 0 members of the (1, 1, λ, 1) triplet of o-$H_2$, respectively, but from the upper state (0, 2, 2, 0) of p-$H_2$. The first two calculated peaks match almost perfectly the experimental features at −7.16 and −6.40 meV (Fig. 6(b)), respectively, and the intensity of the third is probably too small to be measured.

Finally, the prominent peak at −7.79 meV is due to the (1, 0, 1, 1) → (0, 1, 1, 0) transition, from the first excited translational state of p-$H_2$ to the ground TR state of o-$H_2$. Its experimental counterpart is the peak at −8.11 meV (Fig. 6(b)). This is the NE gain partner of the peak at 7.79 meV present in NE loss at low temperature (see Fig. 2(a)).

## IV. CONCLUSIONS

We have performed rigorous quantum simulations of the INS spectra of the prototypical hydrogen endofullerene $H_2@C_{60}$ at several temperatures, which have also been measured by Horsewill and co-workers,[21] and succeeded to clarify and assign all their key features. This computationally extremely demanding objective has been achieved using a highly sophisticated and computationally efficient quantum methodology for the calculation of the INS spectra of a hydrogen molecule confined inside a nanoscale cavity recently developed by us.[22,23] As shown in this work, for higher excitation energies and at higher temperatures, when the transitions are dense, deeper understanding and the assignment of the experimental INS spectra is virtually impossible without accurately calculated energies and intensities of the INS transitions which our theoretical approach provides.

A new selection rule has been derived for the INS spectra of $H_2$ inside $C_{60}$, and more generally, in any near-spherical cavity where the orbital and rotational angular momenta of the guest molecule are coupled. The INS transitions which according to this rule are forbidden have been found to have zero intensity in our computed INS spectra. The newly developed selection rule represents a precedent, as it defies the widely held opinion that the INS spectroscopy of molecular systems is not subject to any selection rule.[12,13] In our opinion, it strongly suggests the existence of similar selection rules in the INS spectroscopy of $H_2$ in $C_{70}$ and possibly on graphene, and of other, more general systems.

The powerful quantum methodology for computing the INS spectra demonstrated in this work is applicable to a wide range of hydrogen-containing systems in chemistry and physics, of fundamental and practical significance. Besides the lower-symmetry $H_2@C_{70}$,[2,37] promising targets include molecular hydrogen in clathrate hydrates,[25,38,39] metal-organic frameworks,[15–17,40,41] and zeolites,[42,43] among others. We also anticipate extensions to nanoconfined polyatomic molecules such as methane[44] and water.[45]

## ACKNOWLEDGMENTS

Z.B. is grateful to the National Science Foundation (NSF) for its partial support of this research through Grant No. CHE-1112292. Z.B. has also been supported by the China 111 Project No. B1202. In addition, the work of Z.B. was supported in part at Technion by a fellowship from the Lady Davis Foundation, and at the Weizmann Intitute of Science by the Joseph Meyerhoff Visiting Professorship. We thank Dr. Daniele Colognesi (CNR, Istituto dei Sistemi

Complessi, Sesto Fiorentino, Italy) and Dr. Stephane Rols and Dr. Jacques Ollivier (Institut Laue-Langevin, Grenoble, France) for providing the experimental resolution functions used in this work.

## APPENDIX A: DERIVATION OF THE INS SELECTION RULE

We consider the p-$H_2$ molecule confined in a near-spherical environment, such as that of $C_{60}$, where its orbital angular momentum $\boldsymbol{l}$ and the rotational angular momentum $\boldsymbol{j}$ couple to give the total angular momentum $\boldsymbol{\lambda}$, with the eigenvalues $\lambda = l + j,\ l + j - 1, \ldots, |l - j|$. The selection rule which we derive here states that *the INS transition involving the ground state* $(0, 0, 0, 0)$ *of* p-$H_2$ *and the excited state* $(n, j, \lambda, l)$ *is* **forbidden** *for* $\boldsymbol{\lambda = j + l - 1}$, *in both NE loss and NE gain.*

The derivation of the above selection rule starts from the spatial component of the INS transition matrix element,[22,23]

$$I_f^i = \left\langle \Psi_f^{5D} \right| \exp(i\vec{\kappa}\cdot\vec{R}_{\rm cm}) \exp\left(i\frac{\vec{\kappa}\cdot\vec{\rho}}{2}\right) \left| \Psi_i^{5D} \right\rangle. \quad \text{(A1)}$$

Here $|\Psi_i^{5D}\rangle$ and $|\Psi_f^{5D}\rangle$ in Eq. (A1) are the 5D eigenstates of the TR Hamiltonian in Eq. (1), representing the spatial parts of the initial ($|i\rangle$) and final states ($|f\rangle$) of the INS transition, respectively. $\vec{R}_{\rm cm}$ is the position vector of the cm of $H_2$, $\vec{\rho}$ is the vector connecting the two H atoms, and $\vec{\kappa}$ is the wave vector of the neutron momentum transfer.[22,23] Also, in the following, $(\theta_R, \phi_R)$ and $(\theta, \phi)$ specify the directions of $\vec{R}_{\rm cm}$ and $\vec{\rho}$, respectively.

We designate the TR eigenstates $|\Psi_\tau^{5D}\rangle$ $(\tau = i, f)$ as $|nj\lambda l, m_\lambda\rangle$ $(-\lambda \le m_\lambda \le \lambda)$,

$$\begin{aligned} \left|\psi_\tau^{5D}\right\rangle &= |nj\lambda l, m_\lambda\rangle = |nl\rangle|j\lambda l, m_\lambda\rangle \\ &= \mathbb{R}_{nl}(R) \sum_{m_l m_j} C_{m_l m_j}^{m_\lambda} |lm_l\rangle|jm_j\rangle \\ &= \mathbb{R}_{nl}(R) \sum_{m_l m_j} C_{m_l m_j}^{m_\lambda} Y_{lm_l}(\theta_R, \phi_R) Y_{jm_j}(\theta, \phi), \end{aligned} \quad \text{(A2)}$$

where $\mathbb{R}_{nl}(R)$ is the radial component the eigenstate of the 3D isotropic HO, with the quantum numbers $n$ and $l$, and $C_{m_l m_j}^{m_\lambda}$ are the Clebsch-Gordan (C-G) coefficients defined in Eq. (B6). Then the initial (ground) state $|\Psi_i^{5D}\rangle$ can be written as

$$\left|\psi_i^{5D}\right\rangle = |0000, 0\rangle = \mathbb{R}_{00}(R) Y_{00}(\theta_R, \phi_R) Y_{00}(\theta, \phi). \quad \text{(A3)}$$

With the help of Eqs. (A2) and (A3), Eq. (A1) can be rewritten as follows:

$$\begin{aligned} I_f^i &= \langle nj\lambda l, m_\lambda| \exp(i\vec{\kappa}\cdot\vec{R}_{\rm cm}) \exp\left(i\frac{\vec{\kappa}\cdot\vec{\rho}}{2}\right) |0000, 0\rangle \\ &= \langle j\lambda l, m_\lambda|\langle nl| \exp(i\vec{\kappa}\cdot\vec{R}_{\rm cm}) \exp\left(i\frac{\vec{\kappa}\cdot\vec{\rho}}{2}\right) |00\rangle|000, 0\rangle. \end{aligned} \quad \text{(A4)}$$

Using Eqs. (30), (31), and (38) in Ref. 23, Eq. (A4) becomes

$$\begin{aligned} I_f^i &= \sum_{LM_L JM_J} i^{L+J} (4\pi)^2 \left( \int_0^\infty dR R^2 \mathbb{R}_{nl}^*(R) \mathbb{R}_{00}(R) j_L(\kappa R) \right) \\ &\quad \times j_J\left(\frac{1}{2}\kappa\rho\right) Y_{LM_L}^*(\theta_{\vec{\kappa}}, \phi_{\vec{\kappa}}) Y_{JM_J}^*(\theta_{\vec{\kappa}}, \phi_{\vec{\kappa}}) \\ &\quad \times \langle j\lambda l, m_\lambda | Y_{LM_L}(\theta_R, \phi_R) Y_{JM_J}(\theta, \phi) | 000, 0\rangle \\ &= \sum_{LM_L JM_J} i^{L+J} (4\pi)^2 \mathbb{T}_L^{00,nl} j_J\left(\frac{1}{2}\kappa\rho\right) \\ &\quad \times Y_{LM_L}^*(\theta_{\vec{\kappa}}, \phi_{\vec{\kappa}}) Y_{JM_J}^*(\theta_{\vec{\kappa}}, \phi_{\vec{\kappa}}) \\ &\quad \times \left( \sum_{m_l m_j} \left(C_{m_l m_j}^{m_\lambda}\right)^* \langle lm_l| \langle jm_j | Y_{LM_L}(\theta_R, \phi_R) \right. \\ &\quad \left. \times Y_{JM_J}(\theta, \phi) |00\rangle |00\rangle \right) \\ &= \sum_{LM_L JM_J} i^{L+J} (4\pi)^2 \mathbb{T}_L^{00,nl} j_J\left(\frac{1}{2}\kappa\rho\right) \\ &\quad \times Y_{LM_L}^*(\theta_{\vec{\kappa}}, \phi_{\vec{\kappa}}) Y_{JM_J}^*(\theta_{\vec{\kappa}}, \phi_{\vec{\kappa}}) \\ &\quad \times \sum_{m_l m_j} \left[ \left(C_{m_l m_j}^{m_\lambda}\right)^* (-1)^{m_l} \left[\frac{(2l+1)(2L+1)}{4\pi}\right]^{\frac{1}{2}} \right. \\ &\quad \times \begin{pmatrix} l & L & 0 \\ 0 & 0 & 0 \end{pmatrix} \begin{pmatrix} l & L & 0 \\ -m_l & M_L & 0 \end{pmatrix} \\ &\quad \times (-1)^{m_j} \left[\frac{(2j+1)(2J+1)}{4\pi}\right]^{\frac{1}{2}} \begin{pmatrix} j & J & 0 \\ 0 & 0 & 0 \end{pmatrix} \\ &\quad \left. \times \begin{pmatrix} j & J & 0 \\ -m_j & M_J & 0 \end{pmatrix} \right] \\ &= i^{l+j} 4\pi \mathbb{T}_l^{00,nl} j_j\left(\frac{1}{2}\kappa\rho\right) \\ &\quad \times \left( \sum_{m_l m_j} C_{m_l m_j}^{m_\lambda} Y_{lm_l}(\theta_{\vec{\kappa}}, \phi_{\vec{\kappa}}) Y_{jm_j}(\theta_{\vec{\kappa}}, \phi_{\vec{\kappa}}) \right)^*, \end{aligned} \quad \text{(A5)}$$

where

$$\mathbb{T}_L^{00,nl} \equiv \int_0^\infty dR R^2 \mathbb{R}_{nl}^*(R) \mathbb{R}_{00}(R) j_L(\kappa R). \quad \text{(A6)}$$

In the above, we set $L = l$, $J = j$, $M_L = m_l$, $M_J = m_j$, based on the following properties of a *non-zero* $3 - j$ symbol $\left(\begin{smallmatrix} J_1 & J_2 & J_3 \\ M_1 & M_2 & M_3 \end{smallmatrix}\right)$:

$$\begin{cases} M_1 + M_2 + M_3 = 0 \\ J_1 + J_2 + J_3 \quad \text{is } integer \\ |M_i| \le J_i \\ |J_1 - J_2| \le J_3 \le J_1 + J_2 \end{cases} \quad \text{(A7)}$$

and

$$\begin{pmatrix} l & l & 0 \\ -m & m & 0 \end{pmatrix} = \frac{(-1)^{l-m}}{\sqrt{2l+1}}. \tag{A8}$$

*To derive the selection rule, one needs to prove that the summation over the spherical harmonics in* Eq. (A5), *is equal to zero for* $\lambda = l + j - 1$, i.e.,

$$\sum_{m_l m_j} C^{m_\lambda}_{m_l m_j} Y_{l m_l}(\theta_{\vec{\kappa}}, \phi_{\vec{\kappa}}) Y_{j m_j}(\theta_{\vec{\kappa}}, \phi_{\vec{\kappa}}) = 0. \tag{A9}$$

This will be done by the *method of induction*. We start by noticing that the above sum corresponds to the right-hand side of Eq. (B6), when the same angular coordinates are used for both $|lm_l\rangle$ and $|jm_j\rangle$ states.

1. $m_\lambda = \lambda = l + j - 1$. Utilizing Eqs. (B5), (C3), (C4), (C6) and (C7), and setting $x \equiv \cos\theta_{\vec{\kappa}}$, we obtain

$$\begin{aligned}
&|\lambda, \lambda\rangle \\
&= \sqrt{\frac{j}{l+j}} Y_{l,l-1}(\theta_{\vec{\kappa}}, \phi_{\vec{\kappa}}) Y_{j,j}(\theta_{\vec{\kappa}}, \phi_{\vec{\kappa}}) \\
&\quad - \sqrt{\frac{l}{l+j}} Y_{l,l}(\theta_{\vec{\kappa}}, \phi_{\vec{\kappa}}) Y_{j,j-1}(\theta_{\vec{\kappa}}, \phi_{\vec{\kappa}}) \\
&= \frac{(-1)^{l+j-1} e^{i(l+j-1)\phi_{\vec{\kappa}}}}{2\pi\sqrt{l+j}} \\
&\quad \times \left( \sqrt{j} P_{l,l-1}(x) P_{j,j}(x) - \sqrt{l} P_{l,l}(x) P_{j,j-1}(x) \right) \\
&= \frac{e^{i(l+j-1)\phi_{\vec{\kappa}}}}{4\pi\sqrt{l+j}} \left[ \frac{(2l+1)(2j+1)}{2(2l-1)!(2j-1)!} \right]^{\frac{1}{2}} \\
&\quad \times \left( P_l^{l-1}(x) P_j^j(x) - P_l^l(x) P_j^{j-1}(x) \right) \\
&= \frac{e^{i(l+j-1)\phi_{\vec{\kappa}}}}{4\pi\sqrt{l+j}} \left[ \frac{(2l+1)(2j+1)}{2(2l-1)!(2j-1)!} \right]^{\frac{1}{2}} \\
&\quad \times \left[ x(-1)^{l-1}(2l-1)!!(1-x^2)^{\frac{l}{2}} (-1)^j (2j-1)!!(1-x^2)^{\frac{j}{2}} \right. \\
&\quad \left. - (-1)^l (2l-1)!!(1-x^2)^{\frac{l}{2}} x (-1)^{j-1} (2j-1)!!(1-x^2)^{\frac{j}{2}} \right] \\
&= 0.
\end{aligned} \tag{A10}$$

2. Let us now assume that Eq. (A9) remains valid, i.e., $|\lambda, m_\lambda\rangle = 0$, for *any* $m_\lambda$ such that $-\lambda < m_\lambda < \lambda$. With the help of Eqs. (C6), (C7), and (B6), and setting $x = \cos\theta_{\vec{\kappa}}$, Eq. (A9) can be rewritten as

$$\sum_{m_l m_j} C^{m_\lambda}_{m_l m_j} \frac{(-1)^{m_\lambda}}{2\pi} e^{i m_\lambda \phi_{\vec{\kappa}}} N_{l,m_l} P_l^{m_l}(\theta_{\vec{\kappa}}) N_{j,m_j} P_j^{m_j}(\theta_{\vec{\kappa}}) = 0 \tag{A11}$$

$$\begin{aligned}
&\Rightarrow \sum_{m_l m_j} C^{m_\lambda}_{m_l m_j} \frac{(-1)^{m_\lambda}}{2\pi} e^{i m_\lambda \phi_{\vec{\kappa}}} N_{l,m_l} N_{j,m_j} \\
&\quad \times \frac{d}{dx} \left( P_l^{m_l}(x) P_j^{m_j}(x) \right) = 0.
\end{aligned} \tag{A12}$$

The normalization constants $N_{l,m_l}$ and $N_{j,m_j}$ are defined by Eqs. (C8) and (C9).

3. Now we must demonstrate that Eq. (A9) holds when $m_\lambda$ is replaced with $m_\lambda - 1$,

$$\sum_{m_l m_j} C^{m_\lambda - 1}_{m_l m_j} Y_{l m_l}(\theta_{\vec{\kappa}}, \phi_{\vec{\kappa}}) Y_{j m_j}(\theta_{\vec{\kappa}}, \phi_{\vec{\kappa}}) = 0. \tag{A13}$$

Using Eq. (B7), Eq. (A13) can be put in the form

$$\begin{aligned}
&\sum_{m_l m_j} C^{m_\lambda - 1}_{m_l m_j} Y_{l m_l}(\theta_{\vec{\kappa}}, \phi_{\vec{\kappa}}) Y_{j m_j}(\theta_{\vec{\kappa}}, \phi_{\vec{\kappa}}) \\
&= \sum_{m_l m_j} \left( \sqrt{\frac{(l+m_l+1)(l-m_l)}{(\lambda+m_\lambda)(\lambda-m_\lambda+1)}} C^{m_\lambda}_{m_l+1, m_j} \right. \\
&\quad \left. + \sqrt{\frac{(j+m_j+1)(j-m_j)}{(\lambda+m_\lambda)(\lambda-m_\lambda+1)}} C^{m_\lambda}_{m_l, m_j+1} \right) \\
&\quad \times Y_{l m_l}(\theta_{\vec{\kappa}}, \phi_{\vec{\kappa}}) Y_{j m_j}(\theta_{\vec{\kappa}}, \phi_{\vec{\kappa}}) \\
&= \sum_{m_l m_j} \sqrt{\frac{(l+m_l+1)(l-m_l)}{(\lambda+m_\lambda)(\lambda-m_\lambda+1)}} C^{m_\lambda}_{m_l+1, m_j} \\
&\quad \times \frac{(-1)^{m_l+m_j}}{2\pi} e^{i(m_l+m_j)\phi_{\vec{\kappa}}} \\
&\quad \times N_{l,m_l} P_l^{m_l}(\theta_{\vec{\kappa}}) N_{j,m_j} P_j^{m_j}(\theta_{\vec{\kappa}}) \\
&\quad + \sum_{m_l m_j} \sqrt{\frac{(j+m_j+1)(j-m_j)}{(\lambda+m_\lambda)(\lambda-m_\lambda+1)}} C^{m_\lambda}_{m_l, m_j+1} \\
&\quad \times \frac{(-1)^{m_l+m_j}}{2\pi} e^{i(m_l+m_j)\phi_{\vec{\kappa}}} \\
&\quad \times N_{l,m_l} P_l^{m_l}(\theta_{\vec{\kappa}}) N_{j,m_j} P_j^{m_j}(\theta_{\vec{\kappa}}).
\end{aligned} \tag{A14}$$

According to Eq. (C5),

$$P_l^m(x) = \frac{\left[ (1-x^2) P_l^{m+1\prime}(x) - (m+1) x P_l^{m+1}(x) \right]}{(l+m+1)(l-m)\sqrt{1-x^2}}$$

$$\Rightarrow \begin{cases} P_l^{m_l}(x) = \dfrac{(1-x^2) P_l^{m_l+1\prime}(x) - (m_l+1) x P_l^{m_l+1}(x)}{(l+m_l+1)(l-m_l)\sqrt{1-x^2}} \\ P_j^{m_j}(x) = \dfrac{(1-x^2) P_j^{m_j+1\prime}(x) - (m_j+1) x P_j^{m_j+1}(x)}{(j+m_j+1)(j-m_j)\sqrt{1-x^2}}. \end{cases} \tag{A15}$$

Using Eqs. (A15) and (C9), and setting $x = \cos\theta_{\vec{\kappa}}$, the first term in Eq. (A14) can be recast as

$$\begin{aligned}
&\sum_{m_l m_j} \sqrt{\frac{(l+m_l+1)(l-m_l)}{(\lambda+m_\lambda)(\lambda-m_\lambda+1)}} C^{m_\lambda}_{m_l+1,m_j} \\
&\quad\times \frac{(-1)^{m_l+m_j}}{2\pi} e^{i(m_l+m_j)\phi_{\vec{\kappa}}} N_{l,m_l} P_l^{m_l}(x) N_{j,m_j} P_j^{m_j}(x) \\
&= \sum_{m_l m_j} \frac{(-1)^{m_l+m_j+1} e^{i(m_l+m_j)\phi_{\vec{\kappa}}}}{2\pi\sqrt{(\lambda+m_\lambda)(\lambda-m_\lambda+1)}\sqrt{1-x^2}} C^{m_\lambda}_{m_l+1,m_j} \\
&\quad\times N_{l,m_l+1}\left[(1-x^2)P_l^{m_l+1\prime}(x) - (m_l+1)x P_l^{m_l+1}(x)\right] \\
&\quad\times N_{j,m_j} P_j^{m_j}(x) \\
&= \sum_{m_l' m_j} \frac{(-1)^{m_l'+m_j} e^{i(m_l'+m_j-1)\phi_{\vec{\kappa}}}}{2\pi\sqrt{(\lambda+m_\lambda)(\lambda-m_\lambda+1)}\sqrt{1-x^2}} C^{m_\lambda}_{m_l',m_j} \\
&\quad\times N_{l,m_l'}\left[(1-x^2)P_l^{m_l''}(x) - m_l' x P_l^{m_l'}(x)\right] N_{j,m_j} P_j^{m_j}(x) \\
&= \sum_{m_l m_j} \frac{(-1)^{m_\lambda} e^{i(m_\lambda-1)\phi_{\vec{\kappa}}}}{2\pi\sqrt{(\lambda+m_\lambda)(\lambda-m_\lambda+1)}\sqrt{1-x^2}} C^{m_\lambda}_{m_l,m_j} \\
&\quad\times N_{l,m_l}\left[(1-x^2)P_l^{m_l\prime}(x) - m_l x P_l^{m_l}(x)\right] N_{j,m_j} P_j^{m_j}(x).
\end{aligned} \tag{A16}$$

In the above, we already set $m_l' = m_l + 1$ in order to change the indices. The second term of Eq. (A14) can be simplified in a similar vein, obtaining

$$\begin{aligned}
&\sum_{m_l m_j} \sqrt{\frac{(j+m_j+1)(j-m_j)}{(\lambda+m_\lambda)(\lambda-m_\lambda+1)}} C^{m_\lambda}_{m_l,m_j+1} \\
&\quad\times \frac{(-1)^{m_l+m_j}}{2\pi} e^{i(m_l+m_j)\phi_{\vec{\kappa}}} N_{l,m_l} P_l^{m_l}(\theta_{\vec{\kappa}}) N_{j,m_j} P_j^{m_j}(\theta_{\vec{\kappa}}) \\
&= \sum_{m_l m_j} \frac{(-1)^{m_\lambda} e^{i(m_\lambda-1)\phi_{\vec{\kappa}}}}{2\pi\sqrt{(\lambda+m_\lambda)(\lambda-m_\lambda+1)}\sqrt{1-x^2}} C^{m_\lambda}_{m_l,m_j} \\
&\quad\times N_{l,m_l} P_l^{m_l}(x) N_{j,m_j}\left[(1-x^2)P_j^{m_j\prime}(x) - m_j x P_j^{m_j}(x)\right].
\end{aligned} \tag{A17}$$

Adding Eqs. (A16) and (A17), one obtains

$$\begin{aligned}
&\frac{e^{-i\phi_{\vec{\kappa}}}\sqrt{1-x^2}}{\sqrt{(\lambda+m_\lambda)(\lambda-m_\lambda+1)}}\left(\sum_{m_l m_j} C^{m_\lambda}_{m_l m_j} \frac{(-1)^{m_\lambda}}{2\pi} e^{i m_\lambda \phi_{\vec{\kappa}}} N_{l,m_l}\right. \\
&\quad\left.\times N_{j,m_j}\frac{d}{dx}\left(P_l^{m_l}(x)P_j^{m_j}(x)\right)\right) \\
&\quad - \frac{e^{-i\phi_{\vec{\kappa}}}x}{\sqrt{(\lambda+m_\lambda)(\lambda-m_\lambda+1)}\sqrt{1-x^2}} \sum_{m_l m_j}(m_l+m_j) C^{m_\lambda}_{m_l m_j} \\
&\quad\times \frac{(-1)^{m_\lambda}}{2\pi} e^{i m_\lambda \phi_{\vec{\kappa}}} N_{l,m_l} P_l^{m_l}(x) N_{j,m_j} P_j^{m_j}(x).
\end{aligned} \tag{A18}$$

The sum in the first term of Eq. (A18) is equal to *zero* because of Eq. (A12). By $m_\lambda = m_l + m_j$ and Eq. (A11), the second term of Eq. (A18) is also *zero*. Therefore, Eq. (A18) is *zero*, which proves that Eq. (A13) is correct. Thus, we have proved Eq. (A9) by induction. Equation (A5) is therefore equal to zero for the transitions between the ground TR state (0, 0, 0, 0) and excited TR states $(n, j, \lambda, l)$ when $\lambda = l + j - 1$ (for all possible $m_\lambda$). This concludes our derivation of the selection rule.

## APPENDIX B: GENERATING THE TOTAL ANGULAR MOMENTUM EIGENVECTORS $|\lambda, m_\lambda\rangle$

Let $\hat{\lambda} \equiv \hat{l} + \hat{j}$ and $\hat{\lambda}_\pm = \hat{l}_\pm + \hat{j}_\pm$. The following expression will be required in the derivation:

$$\begin{aligned}
&\hat{J}_\pm |J_i M_i\rangle = \sqrt{(J_i \mp M_i)(J_i \pm M_i + 1)}\,|J_i M_i \pm 1\rangle, \\
&\qquad \hat{J} \equiv \hat{\lambda}, \hat{l}, \text{ or } \hat{j}.
\end{aligned} \tag{B1}$$

### 1. $\lambda = l + j$

The initial vector is $|\lambda = l + j, m_\lambda = \lambda\rangle \equiv |l, m_l = l\rangle |j, m_j = j\rangle$. Then,

$$\begin{aligned}
\hat{\lambda}_-|\lambda,\lambda\rangle &= \sqrt{(\lambda+\lambda)(\lambda-\lambda+1)}|\lambda,\lambda-1\rangle = \sqrt{2\lambda}|\lambda,\lambda-1\rangle \\
&= (\hat{l}_- + \hat{j}_-)|l,l\rangle|j,j\rangle = \sqrt{(l+l)(l-l+1)}|l,l-1\rangle|j,j\rangle \\
&\quad + \sqrt{(j+j)(j-j+1)}|l,l\rangle|j,j-1\rangle \\
&= \sqrt{2l}|l,l-1\rangle|j,j\rangle + \sqrt{2j}|l,l\rangle|j,j-1\rangle \\
&\Rightarrow |\lambda,\lambda-1\rangle = \sqrt{\frac{l}{\lambda}}|l,l-1\rangle|j,j\rangle + \sqrt{\frac{j}{\lambda}}|l,l\rangle|j,j-1\rangle.
\end{aligned} \tag{B2}$$

By repeated application of $\hat{\lambda}_-$ to Eq. (B2) one can generate all of vectors $|\lambda, m_\lambda\rangle$, where $\lambda = l + j$ and $m_\lambda = \lambda, \lambda - 1, \ldots, -\lambda$.

### 2. $\lambda = l + j - 1$

The eigenvector $|\lambda = l + j - 1, m_\lambda = l + j - 1\rangle$ is generated starting from Eq. (B2) and imposing the orthogonality and normalization conditions

$$\langle l+j, l+j-1|l+j-1, l+j-1\rangle = 0, \tag{B3}$$

$$\langle l+j-1, l+j-1|l+j-1, l+j-1\rangle = 1. \tag{B4}$$

One obtains

$$\begin{aligned}
|l+j-1, l+j-1\rangle &= \sqrt{\frac{j}{l+j}}|l,l-1\rangle|j,j\rangle \\
&\quad - \sqrt{\frac{l}{l+j}}|l,l\rangle|j,j-1\rangle.
\end{aligned} \tag{B5}$$

Repeated application of $\hat{\lambda}_-$ to Eq. (B5) yields all of the vectors $|\lambda, m_\lambda\rangle$, where $\lambda = l + j - 1$ and $m_\lambda = \lambda, \lambda - 1, \ldots, -\lambda$.

### 3. Clebsch-Gordan coefficients

In terms of the C-G coefficients, $|\lambda, m_\lambda\rangle$ can be written as

$$|\lambda, m_\lambda\rangle = \sum_{m_l m_j} C^{m_\lambda}_{m_l m_j} |l m_l\rangle |j m_j\rangle, \quad m_\lambda = m_l + m_j. \tag{B6}$$

By applying $\hat{\lambda}_-$ to both sides of Eq. (B6), the following recursion expression is obtained linking $|\lambda, m_\lambda - 1\rangle$ and $|\lambda, m_\lambda\rangle$, for $-\lambda < m_\lambda \leq \lambda$,

$$C^{m_\lambda - 1}_{m_l m_j} = \sqrt{\frac{(l + m_l + 1)(l - m_l)}{(\lambda + m_\lambda)(\lambda - m_\lambda + 1)}} C^{m_\lambda}_{m_l + 1, m_j} + \sqrt{\frac{(j + m_j + 1)(j - m_j)}{(\lambda + m_\lambda)(\lambda - m_\lambda + 1)}} C^{m_\lambda}_{m_l, m_j + 1}. \tag{B7}$$

## APPENDIX C: FORMULAE HELPFUL FOR DERIVING THE SELECTION RULE

The following definitions and relationships involving the associated Legendre polynomials[46] are used in the derivation of the selection rule.

1. Definition in terms of the ordinary Legendre polynomials $P_l(x)$:
   (a) non-negative $m$:

$$P_l^m(x) = (-1)^m (1 - x^2)^{\frac{m}{2}} \frac{d^m}{dx^m} P_l(x) = \frac{(-1)^m}{2^l l!} (1 - x^2)^{\frac{m}{2}} \frac{d^{l+m}}{dx^{l+m}} (x^2 - 1)^l. \tag{C1}$$

   (b) negative $m = -|m|$:

$$P_l^{-|m|}(x) = (-1)^m \frac{(l - |m|)!}{(l + |m|)!} P_l^{|m|}(x). \tag{C2}$$

2. Helpful identities:

$$P_l^l(x) = (-1)^l (2l - 1)!! (1 - x^2)^{\frac{l}{2}}, \tag{C3}$$

$$P_{l+1}^l(x) = x(2l + 1) P_l^l(x) = x(-1)^l (2l + 1)!! (1 - x^2)^{\frac{l}{2}}. \tag{C4}$$

3. Recurrence formula:

$$(x^2 - 1) P_l^{m+1\prime}(x) = -(l + m + 1)(l - m) \times \sqrt{1 - x^2} P_l^m(x) - (m + 1) x P_l^{m+1}(x). \tag{C5}$$

Several useful formulae involving the spherical harmonics[46] are also listed here for easy reference

$$Y_{lm}(\theta, \phi) = (-1)^m P_{l,m}(\theta) \frac{1}{\sqrt{2\pi}} e^{im\phi}, \tag{C6}$$

where $P_{l,m}(\theta)$ are the standard, normalized associated Legendre functions. They have the following property:

$$P_{l,m}(\theta) = \begin{cases} (-1)^m \left[\frac{(2l + 1)}{2} \frac{(l - m)!}{(l + m)!}\right]^{\frac{1}{2}} P_l^m(\theta) & m \geq 0 \\ (-1)^m P_{l,|m|}(\theta) & m < 0 \end{cases} \equiv N_{l,m} P_l^m(\theta). \tag{C7}$$

$N_{l,m}$ above is the normalization constant

$$N_{l,m} = (-1)^m \left[\frac{(2l + 1)}{2} \frac{(l - m)!}{(l + m)!}\right]^{\frac{1}{2}} \tag{C8}$$

$$\Rightarrow N_{l,m} = -\sqrt{(l - m)(l + m + 1)} N_{l,m+1}. \tag{C9}$$

Finally,

$$Y^*_{lm}(\theta, \phi) = (-1)^m Y_{l,-m}(\theta, \phi). \tag{C10}$$


[1] S. Mamone, J. Y.-C. Chen, R. Bhattacharyya, M. H. Levitt, R. G. Lawler, A. J. Horsewill, T. Rõõm, Z. Bačić, and N. J. Turro, Coord. Chem. Rev. **255**, 938 (2011).
[2] M. Xu, F. Sebastianelli, B. R. Gibbons, Z. Bačić, R. Lawler, and N. J. Turro, J. Chem. Phys. **130**, 224306 (2009).
[3] M. Ge, U. Nagel, D. Hüvonen, T. Rõõm, S. Mamone, M. H. Levitt, M. Carravetta, Y. Murata, K. Komatsu, J. Y.-C. Chen, and N. J. Turro, J. Chem. Phys. **134**, 054507 (2011).
[4] M. Xu, F. Sebastianelli, Z. Bačić, R. Lawler, and N. J. Turro, J. Chem. Phys. **128**, 011101 (2008).
[5] M. Xu, F. Sebastianelli, Z. Bačić, R. Lawler, and N. J. Turro, J. Chem. Phys. **129**, 064313 (2008).
[6] S. Mamone, M. Ge, D. Hüvonen, U. Nagel, A. Danquigny, F. Cuda, M. C. Grossel, Y. Murata, K. Komatsu, M. H. Levitt, T. Rõõm, and M. Carravetta, J. Chem. Phys. **130**, 081103 (2009).
[7] M. Ge, U. Nagel, D. Hüvonen, T. Rõõm, S. Mamone, M. H. Levitt, M. Carravetta, Y. Murata, K. Komatsu, X. Lei, and N. J. Turro, J. Chem. Phys. **135**, 114511 (2011).
[8] M. Carravetta, O. G. Johannessen, M. H. Levitt, I. Heinmaa, R. Stern, A. Samoson, A. J. Horsewill, Y. Murata, and K. Komatsu, J. Chem. Phys. **124**, 104507 (2006).
[9] M. Carravetta, A. Danquigny, S. Mamone, F. Cuda, O. G. Johannessen, I. Heinmaa, K. Panesar, R. Stern, M. C. Grossel, A. J. Horsewill, A. Samoson, M. Murata, Y. Murata, K. Komatsu, and M. H. Levitt, Phys. Chem. Chem. Phys. **9**, 4879 (2007).
[10] K. Komatsu, M. Murata, and Y. Murata, Science **307**, 238 (2005).
[11] M. Murata, Y. Murata, and K. Komatsu, J. Am. Chem. Soc. **128**, 8024 (2006).
[12] A. J. Ramirez-Cuesta, M. J. Jones, and W. I. F. David, Mater. Today **12**(11), 54 (2009).
[13] G. J. Kearley and M. R. Johnson, Vib. Spectrosc. **53**, 54 (2010).
[14] G. L. Squires, *Introduction to the Theory of Thermal Neutron Scattering* (Dover Press, New York, 1996).
[15] J. L. C. Rowsell, J. Eckert, and O. M. Yaghi, J. Am. Chem. Soc. **127**, 14904 (2005).
[16] F. M. Mulder, T. J. Dingemans, H. G. Schimmel, A. J. Ramirez-Cuesta, and G. J. Kearley, Chem. Phys. **351**, 72 (2008).
[17] C. M. Brown, Y. Liu, T. Yildirim, V. K. Peterson, and C. J. Kepert, Nanotechnology **20**, 204025 (2009).
[18] L. Kong, G. Román-Peréz, J. M. Soler, and D. C. Langreth, Phys. Rev. Lett. **103**, 096103 (2009).
[19] A. J. Horsewill, K. S. Panesar, S. Rols, M. R. Johnson, Y. Murata, K. Komatsu, S. Mamone, A. Danquigny, F. Cuda, S. Maltsev, M. C. Grossel, M. Carravetta, and M. H. Levitt, Phys. Rev. Lett. **102**, 013001 (2009).
[20] A. J. Horsewill, S. Rols, M. R. Johnson, Y. Murata, M. Murata, K. Komatsu, M. Carravetta, S. Mamone, M. H. Levitt, J. Y.-C. Chen, J. A. Johnson, X. Lei, and N. J. Turro, Phys. Rev. B **82**, 081410(R) (2010).

[21]A. J. Horsewill, K. S. Panesar, S. Rols, J. Ollivier, M. R. Johnson, M. Carravetta, S. Mamone, M. H. Levitt, Y. Murata, K. Komatsu, J. Y.-C. Chen, J. A. Johnson, X. Lei, and N. J. Turro, Phys. Rev. B **85**, 205440 (2012).
[22]M. Xu, L. Ulivi, M. Celli, D. Colognesi, and Z. Bačić, Phys. Rev. B **83**, 241403(R) (2011).
[23]M. Xu and Z. Bačić, Phys. Rev. B **84**, 195445 (2011).
[24]M. Xu, L. Ulivi, M. Celli, D. Colognesi, and Z. Bačić, Chem. Phys. Lett. **563**, 1 (2013).
[25]M. Xu, Y. Elmatad, F. Sebastianelli, J. W. Moskowitz, and Z. Bačić, J. Phys. Chem. B **110**, 24806 (2006).
[26]M. Xu, F. Sebastianelli, and Z. Bačić, J. Chem. Phys. **128**, 244715 (2008).
[27]M. Xu, F. Sebastianelli, and Z. Bačić, J. Phys. Chem. A **113**, 7601 (2009).
[28]S. Ye, M. Xu, Z. Bačić, R. Lawler, and N. J. Turro, J. Phys. Chem. A **114**, 9936 (2010).
[29]K. Hedberg, L. Hedberg, D. S. Bethune, C. A. Brown, H. C. Dorn, R. D. Johnson, and M. de Vries, Science **254**, 410 (1991).
[30]S. Liu, Z. Bačić, J. W. Moskowitz, and K. E. Schmidt, J. Chem. Phys. **103**, 1829 (1995).
[31]Z. Bačić and J. C. Light, Annu. Rev. Phys. Chem. **40**, 469 (1989).
[32]H. Stein, H. Stiller, and R. Stockmeyer, J. Chem. Phys. **57**, 1726 (1972).
[33]S. W. Lovesey, *Theory of Neutron Scattering from Condensed Matter* (Oxford University Press, Oxford, 1984), Vol. 1.
[34]D. Colognesi, M. Celli, L. Ulivi, M. Xu, and Z. Bačić, "Neutron scattering measurements and computation of the quantum dynamics of hydrogen molecules trapped in the small and large cages of clathrate hydrates," J. Phys. Chem. A (published online).
[35]J. M. Perez-Mato, M. Aroyo, J. Hlinka, M. Quilichini, and R. Currat, Phys. Rev. Lett. **81**, 2462 (1998).
[36]R. J. Elliott and M. F. Thorpe, Proc. Phys. Soc. **91**, 903 (1967).
[37]F. Sebastianelli, M. Xu, Z. Bačić, R. Lawler, and N. J. Turro, J. Am. Chem. Soc. **132**, 9826 (2010).
[38]L. Ulivi, M. Celli, A. Giannasi, A. J. Ramirez-Cuesta, D. J. Bull, and M. Zoppi, Phys. Rev. B **76**, 161401(R) (2007).
[39]K. T. Tait, F. Trouw, Y. Zhao, C. M. Brown, and R. T. Downs, J. Chem. Phys. **127**, 134505 (2007).
[40]P. D. C. Dietzel, P. A. Georgiev, J. Eckert, R. Blom, T. Strässle, and T. Unruh, Chem. Commun. **46**, 4962 (2010).
[41]I. Matanović, J. L. Belof, B. Space, K. Sillar, J. Sauer, J. Eckert, and Z. Bačić, J. Chem. Phys. **137**, 014701 (2012).
[42]P. A. Georgiev, A. Albinati, B. L. Mojet, J. Ollivier, and J. Eckert, J. Am. Chem. Soc. **129**, 8086 (2007).
[43]J. M. Nicol, J. Eckert, and J. Howard, J. Phys. Chem. **92**, 7117 (1988).
[44]I. Matanović, M. Xu, J. W. Moskowitz, J. Eckert, and Z. Bačić, J. Chem. Phys. **131**, 224308 (2009).
[45]K. Kurotobi and Y. Murata, Science **333**, 613 (2011).
[46]G. Arfken, *Mathematical Methods for Physicists* (Academic Press, Orlando, FL, 1985).